Random force identification via Kalman filtering on a cantilevered structure

R. Álvarez-Briceño [1], **L. P. R. de Oliveira** [1]
[1] Mechanical Engineering Department, São Carlos School of Engineering, University of São Paulo,
Av. Trabalhador São Carlense, 400, Parque Arnold Schmidt,
São Carlos, São Paulo, CEP 13566-590, Brazil.
e-mail: **leopro@sc.usp.br**

Abstract
Several engineering applications demand in-operation dynamic forces exerted on structural component to be modeled. Although direct input measurements would be the first option to solve this lack, in many instances an appropriate and feasible instrumentation is hard to be accomplished due to reduced space, especial environment conditions, etc. New methods have to be explored to solve instrument limitations. In the field of virtual sensing, augmented-state Kalman Filter (AKF) based techniques have recently been introduced in the field of force estimation. The ability of the AKF for predicting a point force random in time, based only on accelerometer measurements, is evaluated experimentally in the present work. The present experimental approach features a cantilevered structure, instrumented with two pairs of accelerometers, mounted approximately at its mid-length and at its free tip. A force sensor is used to measure the actual input force on the beams free end. Measured and predicted force time histories show a good agreement.

1 Introduction

Shell-and-tube heat exchangers are the most common type of heat exchanger found in industrial processes [1]. These devices are also used in more complex systems, for example, in pressurized water reactors of nuclear power plants, which represent a critical application since a mechanical failure implies significant economical losses, unexpected shut downs, not to mention critical radioactive accidents. In this sense, design engineers must take care not only of thermohydraulic efficiency but also of the structural integrity of the heat exchanger. Flow-induced vibration (FIV) is the most important dynamic issue in the design of heat exchangers. Furthermore, almost half of all shell-and-tube heat exchangers in the industry operate under two-phase flow condition in the shell side [2, 3], which corresponds to a more critical condition for FIV if compared with the single-phase flow case. Therefore, the experimental database that can be obtained on FIV is key to understand the phenomena and develop design guidelines to avoid extreme conditions that may shorten the apparatus lifetime.

In two-phase crossflow conditions, there are four types of vibration mechanisms that may take place in the tube bundle, namely: (i) fluidelastic instability, (ii) vortex shedding, (iii) turbulence-induced excitation and (iv) acoustic resonance, their definitions are detailed in many references [4, 5, 6, 7, 8]. According to Pettigrew et al. [9], fluidelastic instability and turbulence-induced excitation are the most important vibration mechanisms in tube bundles during two-phase crossflow, while periodic shedding and acoustic resonance are unlikely to occur.

Although there are some design guidelines to estimate the vibration amplitude in turbulence-induced vibration [10, 11, 12], the database about this phenomenon is limited if compared to that available for fluidelastic instability mechanism. This is somewhat surprising since the turbulence-induced vibration mechanism in

tube bundles cannot be avoided, and can only be due to the challenges imposed by both, theoretical and experimental approaches, in tackling this problem. Further, this vibration mechanism is a *necessary evil* since it helps to improve heat transfer through the external fluid. On the other hand, turbulence-induced vibration without supervision may generate fretting wear between tubes and fatigue of structural components, thereby shortening heat exchanger lifetime. In this sense, a deeper knowledge on the turbulence-induced vibration mechanism would help in designing tasks, leading to enhanced heat exchanger performance and security. For this, further experimental studies on this vibration mechanism are required, mainly when it comes to identifying the nature of loads acting on such structures. However, an appropriate instrumentation is hard to be accomplished, mainly due to reduced spaces in tube bundles and because typical instruments are hardly liquid resistant.

In recent years, virtual sensing has arisen as a solution for determining forces when direct measurements are not feasible or present important technical challenges. Virtual sensors, based on a previously modeled system, take readings from real physical sensors to calculate the desired outputs by using some process models [13, 14]. Moreover, these readings are used to get the system model continuously updated, thus model imperfections or non considered in-operating modifications are taken into account for every time instant. This feature enables the assessment of uncertain parameters or variabilities within the system [15], which, with the present application in mind, could mean tracking dynamic changes in the tube bundles promoted by the surrounding fluid and flow conditions and flow - induced forces.

Recently, deterministic - stochastic methods have attracted more attention of researchers since these methods can be used to model the noise as stochastic processes and assume that noise is present not only on the measurements, but also on the state variables, which is a feature that set them apart from purely deterministic techniques. Furthermore, they differ from purely stochastic techniques because force values are still considered to be deterministic quantities [16]. In this context, Kalman filtering (KF) [17, 18] based techniques have been introduced in the field of force estimation. This method provides a particularly practical and efficient state estimation algorithm for linear systems which leads to an optimal result with respect to the expected error covariance [19]. In order to do that, the approach adopted by some authors [20, 16, 15, 19] is to implement a coupled state - disturbance - parameter estimator based on a state-augmented Kalman filter (AKF). In other words, the regular states are augmented with the unknown forces in order to estimate them together [16]. Such kind of estimator is needed in order to distinguish whether changes in time history result from inherent system dynamics or external excitation [14].

The AKF algorithm stability and methods to avoid divergence on estimates are currently being discussed [16, 19]. For instance, Naets et al. [19] propose the addition of displacement dummy measurements for all the degrees of freedom (DOF) in order to prevent drift on predictions. Moreover, one of the most important questions to be clarified in this matter is what type of forces can be estimated reasonably via AKF algorithm. In this context, Berg and Keith Miller [20] implemented the AKF algorithm to estimate random wind loads, while Lourens et al. [16] used the method to predict impulse and sine-sweep forces, showing acceptable results in both cases. Naets et al. [15] tested the AKF algorithm for the identification of an impulsive force applied on a beam free-end, showing good results. In this context, it is expected that the flow turbulence delivers a random in time force to the tube, therefore it is worth testing if the AKF-DM algorithm is able to predict this kind of force. Thus, a structure can be immersed in a two-phase flow aiming to estimate flow-induced forces based on its acceleration response.

The present work focuses on checking the validity of the AKF-DM algorithm to estimate a known point force, which is applied at the free end of a cantilever structure. The applied force is random in time, whose prediction represents a new challenge for this kind of approach. As the aim of this study is to validate a concept for turbulence-induced vibration under two-phase flow, the structure is mounted on a heat exchanger mock-up, which mimics the same boundary conditions that the structure will present in the actual test section. Moreover, the structure is designed so that future tests in two-phase flow can be performed. The remainder of this document is organized as such: the next section present the formulation of the Kalman filter and the necessary modifications to grant stability to the process. Next, a description of the test set-up is presented and the system's identification via Experimental Modal Analysis (EMA) is detailed. Finally, the AKF-DM

algorithm is implemented to estimate the input force, then the results are discussed and compared with measured data.

2 Augmented Kalman filter and dummy measurements for force estimation

This section is devoted to define the formulation used in the implementation of the AKF-DM algorithm. First, since the present analysis is performed on an existent physical system, the modeling equations are expressed in terms of the modal space representation. Subsequently, the discrete state space notation is introduced, which is helpful in the KF algorithm definition. After that, some modifications on KF formulation are proposed in order to obtain the AKF algorithm. Finally, the inclusion of displacement dummy measurements in the algorithm is explained and implemented.

2.1 State equations for the mechanical system

Mechanical systems can be formulated in several ways, including those based on experimental results, such as Experimental Modal Analysis (EMA) procedure. After the corresponding tests are performed, and under the assumptions that the system is Linear Time - Invariant (LTI) with proportional damping, related algorithms are used to obtain the system modal matrix $\mathbf{\Psi}$, undamped natural frequencies ω_n, and damping ratios ζ_n. This set of data enables the derivation of a completely defined modal model of the system.

In order to define the system in physical generalized coordinates [1], the following equations can be used to calculate the mass $\mathbf{M}$, stiffness $\mathbf{K}$, and damping $\mathbf{C}$ matrices, respectively [21]:

$$\mathbf{M} = \mathbf{\Psi}^{-T}\mathbf{\Psi}^{-1}, \tag{1}$$

$$\mathbf{K} = \mathbf{\Psi}^{-T}\begin{bmatrix} \ddots & & \\ & \omega_r^2 & \\ & & \ddots \end{bmatrix}\mathbf{\Psi}^{-1}, \tag{2}$$

$$\mathbf{C} = \mathbf{\Psi}^{-T}\begin{bmatrix} \ddots & & \\ & 2\zeta_r\omega_r & \\ & & \ddots \end{bmatrix}\mathbf{\Psi}^{-1}, \tag{3}$$

where r denotes the r-th vibration mode. Matrices $\mathbf{M}$, $\mathbf{C}$ and $\mathbf{K}$ characterize the system in its spatial model defined by the system of second - order differential equations

$$\mathbf{M}\ddot{\xi} + \mathbf{C}\dot{\xi} + \mathbf{K}\xi = \mathbf{b}\mathbf{f} + \mathbf{b_d}\mathbf{f_d}, \tag{4}$$

where ξ is the vector of physical generalized coordinates. The terms $\mathbf{f}$ and $\mathbf{f_d}$ represent the forces and unknown disturbances, which are applied on the system at positions coordinates described by the selection matrices $\mathbf{b}$ and $\mathbf{b_d}$, respectively.

Mechanical systems can also be represented as a system of first order differential equations, which is referred to as state space model [22]. In the same way, for a LTI system, Eq. 4 can be written as:

$$\dot{\mathbf{x}}(t) = \mathbf{A}\mathbf{x}(t) + \mathbf{B}\mathbf{u}(t) + \mathbf{B_1}\mathbf{w}(t), \tag{5}$$

with measurements

$$\mathbf{y}(t) = \mathbf{H}\mathbf{x}(t) + \mathbf{v}(t), \tag{6}$$

[1] In this case, physical generalized coordinates are preferred over modal coordinates since it facilitates the choose of displacement dummy measurements in further sections

where $\mathbf{x}(t)$ is the state vector, $\mathbf{u}(t)$ is the known control inputs vector, $\mathbf{y}(t)$ represent the sensor outputs vector, and $\mathbf{w}(t)$ and $\mathbf{v}(t)$ are the process and measurement noise, which are assumed as stochastic processes [16].

The state matrix $\mathbf{A}$, the input matrix $\mathbf{B}$ and input disturbance matrix $\mathbf{B_1}$ are formulated in terms of the system's mass, stiffness and damping as follows:

$$\mathbf{A} = \begin{bmatrix} 0 & \mathbf{I} \\ -\mathbf{M}^{-1}\mathbf{K} & -\mathbf{M}^{-1}\mathbf{C} \end{bmatrix} \qquad \mathbf{B} = \begin{bmatrix} 0 \\ \mathbf{M}^{-1}\mathbf{b} \end{bmatrix} \qquad \mathbf{B_1} = \begin{bmatrix} 0 \\ \mathbf{M}^{-1}\mathbf{b_d} \end{bmatrix} \tag{7}$$

The measurement matrix, $\mathbf{H}$, is used to theoretically formulate the measurements as a linear combination of the states at a given time. The measurement matrix will be formulated further for an augmented-state formulation.

The state space nomenclature given by Eqs. 5 and 6 is derived in continuous time domain. However, the simulation analysis using the KF algorithm is performed by sampling the system dynamics at regular time intervals, therefore it is convenient to define the system equations in the discrete time domain. In this manner, these differential equations can be expressed as recursive difference equations [23]

$$\mathbf{x}(k+1) = \mathbf{\Phi}\mathbf{x}(k) + \mathbf{\Gamma}\mathbf{u}(k) + \mathbf{\Gamma_1}\mathbf{w}(k), \tag{8}$$

with measurements

$$\mathbf{y}(k) = \mathbf{H}\mathbf{x}(k) + \mathbf{v}(k), \tag{9}$$

where $\mathbf{\Phi}$, $\mathbf{\Gamma}$ and $\mathbf{\Gamma_1}$ are the discrete versions of matrices $\mathbf{A}$, $\mathbf{B}$ and $\mathbf{B_1}$, respectively. There are some methods to convert continuous system matrices in their discrete - time versions that have already been implemented in MATLAB ®. In the present study, the zero-order hold (ZOH) method is adopted.

Regarding the properties of process and measurement noise, $\mathbf{w}(k)$ and $\mathbf{v}(k)$, respectively, it can be assumed that they are random stationary sequences, mutually uncorrelated, with zero mean, that is:

$$\mathbf{E}\left\{\mathbf{w}(k)\right\} = \mathbf{E}\left\{\mathbf{v}(k)\right\} = 0,$$

have no time correlation or are "white" noise, that is:

$$\mathbf{E}\left\{\mathbf{w}(i)\mathbf{w}^T(j)\right\} = \mathbf{E}\left\{\mathbf{v}(i)\mathbf{v}^T(j)\right\} = 0 \qquad \text{if} \quad i \neq j,$$

and their covariances or mean square "noise levels" are defined by

$$\mathbf{E}\left\{\mathbf{w}(k)\mathbf{w}^T(k)\right\} = \mathbf{R_w}, \qquad \mathbf{E}\left\{\mathbf{v}(k)\mathbf{v}^T(k)\right\} = \mathbf{R_v}.$$

as detailed in [23] and acknowledged in references [20, 16, 19].

2.2 Kalman filter equations

The Kalman filter [17, 18] can be defined as a recursive linear state estimator designed to be optimal in a minimum - variance unbiased sense [16].

The main feature of Kalman filtering is the propagation of the covariance of the state estimates, $\mathbf{P}$ [19]. The basic idea behind this algorithm is to calculate the best state estimate $\hat{\mathbf{x}}(k)$, by combining a previous estimate $\bar{\mathbf{x}}(k)$ with the current measurement $\bar{\mathbf{y}}(k)$, based on the relative accuracy of both, which is in terms of the covariance of the prior estimate, $\mathbf{G}(k)$, and the covariance of the current measurement $\mathbf{R_v}$. Furthermore, the other key idea is to use the known dynamics of $\mathbf{x}$ to predict its behavior in order to estimate $\bar{\mathbf{x}}(k)$ given $\hat{\mathbf{x}}(k-1)$ [23].

The discrete KF algorithm can be arranged in two-stages: measurement update and time update. Based on [23], a summary of the required relations is:

- At the measurement time (measurement update)

$$\hat{\mathbf{x}}(k) = \bar{\mathbf{x}}(k) + \mathbf{P}(k)\mathbf{H}^T\mathbf{R}_\mathbf{v}^{-1}\left(\mathbf{y}(k) - \mathbf{H}\bar{\mathbf{x}}(k)\right), \tag{10}$$

where

$$\mathbf{P}(k) = \mathbf{G}(k) - \mathbf{G}(k)\mathbf{H}^T\left(\mathbf{H}\mathbf{G}(k)\mathbf{H}^T + \mathbf{R}_\mathbf{v}\right)^{-1}\mathbf{H}\mathbf{G}(k). \tag{11}$$

- Between measurements (time update)

$$\bar{\mathbf{x}}(k+1) = \mathbf{\Phi}\hat{\mathbf{x}}(k) + \mathbf{\Gamma}\mathbf{u}(k), \tag{12}$$

and

$$\mathbf{G}(k+1) = \mathbf{\Phi}\mathbf{P}(k)\mathbf{\Phi}^T + \mathbf{\Gamma_1}\mathbf{R_w}{\mathbf{\Gamma_1}}^T, \tag{13}$$

where the initial conditions for $\bar{\mathbf{x}}(0)$ and $\mathbf{G}(0)$ must be assumed to be some value for initialization.

2.3 Augmented Kalman filter for input estimation

The discrete Kalman filter algorithm can be rearranged in order to allow the coupled state - disturbance estimation. For that purpose, the input vector is included in the state vector. However, as it was noted by Naets et al. [19] and Berg and Keith Miller [20], the dynamics relating $\dot{\mathbf{u}}$ to the new state vector, now composed by ξ, $\dot{\xi}$ and $\mathbf{u}$, are likely unknown. This lack of knowledge can be modeled setting:

$$\dot{\mathbf{u}}(t) = 0 + \mathbf{z}(t), \tag{14}$$

where $\mathbf{z}$ is a random vector, thus making $\mathbf{u}$ constant except for model uncertainty. In this manner, Eq. 8 can be rearranged as [20]:

$$\begin{gathered}\begin{bmatrix}\mathbf{x}(k+1)\\ \mathbf{u}(k+1)\end{bmatrix} = \begin{bmatrix}\mathbf{\Phi} & \mathbf{\Gamma}\\ 0 & \mathbf{L}\end{bmatrix}\begin{bmatrix}\mathbf{x}(k)\\ \mathbf{u}(k)\end{bmatrix} + \begin{bmatrix}\mathbf{\Gamma_1} & 0\\ 0 & \Delta t\mathbf{L}\end{bmatrix}\begin{bmatrix}\mathbf{w}(k)\\ \mathbf{z}(k)\end{bmatrix},\\ \begin{bmatrix}\mathbf{w}(k)\\ \mathbf{z}(k)\end{bmatrix} \sim N\left(0, \begin{bmatrix}\mathbf{R_w} & 0\\ 0 & \mathbf{R_z}\end{bmatrix}\right)\end{gathered} \tag{15}$$

where Δt is the time step and $\mathbf{L}$ must be set according to the position where the force is applied. Furthermore, in the case of acceleration measurements on each DOF, the measurements equation is given by [19]

$$\mathbf{y}(k) = \begin{bmatrix}-\mathbf{M^{-1}K} & -\mathbf{M^{-1}C} & \mathbf{M^{-1}b}\end{bmatrix}\begin{bmatrix}\mathbf{x}(k)\\ \mathbf{u}(k)\end{bmatrix} + \mathbf{v}(k), \quad \mathbf{v}(k) \sim N\left(0, \mathbf{R_v}\right) \tag{16}$$

In this manner, the AKF for coupled state - disturbance excitation can be implemented by substituting the non-starred matrices by the starred ones in Eqs. 10 - 13:

$$\begin{gathered}\mathbf{\Phi}^\star = \begin{bmatrix}\mathbf{\Phi} & \mathbf{\Gamma}\\ 0 & \mathbf{L}\end{bmatrix}, \quad \mathbf{\Gamma}^\star = 0, \quad \mathbf{\Gamma_1^\star} = \begin{bmatrix}\mathbf{\Gamma_1} & 0\\ 0 & \Delta t\mathbf{L}\end{bmatrix},\\ \mathbf{R_w^\star} = \begin{bmatrix}\mathbf{R_w} & 0\\ 0 & \mathbf{R_z}\end{bmatrix}, \quad \mathbf{H}^\star = \begin{bmatrix}-\mathbf{M^{-1}K} & -\mathbf{M^{-1}C} & \mathbf{M^{-1}b}\end{bmatrix}\end{gathered} \tag{17}$$

2.4 Dummy measurements implementation in augmented Kalman filter algorithm

Aiming at stable simulations and trying to maintain a generally applicable approach for coupled state/input force estimation, that relies only on acceleration measurements, Naets et al. [19] propose to add displacement dummy measurements for the positions in which the acceleration response is measured. This AKF-DM algorithm was validated via numerical and experimental procedures in [19]. It was found that the inclusion of such dummy measurements to the AKF algorithm (AKF-DM) present stable and consistent results on force predictions, while force estimation through regular AKF diverges from the real force values over longer estimation periods. This is a solution similar to that initially proposed by Chatzi and Fuggini [32] for civil structure monitoring purposes. They indicate that this artifice is plausible since, in structural systems, the deformation of the structure is bounded and it can typically be estimated a priori via analytical models or finite element models. In this way, the estimated deformation can then be considered as the uncertainty on a dummy measurement with an actual zero value [19].

The displacement dummy measurements have equations

$$\mathbf{H_{dm}x} + \mathbf{v_{dm}} = 0, \tag{18}$$

with

$$\mathbf{H_{dm}} = \begin{bmatrix} \mathbf{I}_n & 0 & 0 \end{bmatrix}. \tag{19}$$

Equation 18 states that the position of the DOF is zero with an uncertainty $\mathbf{v_{dm}}$ with covariance $\mathbf{R_{dm}}$. Moreover, the entries of $\mathbf{R_{dm}}$ can be used for the tuning of the KF. In this context, Naets et al. [19] suggest that displacement dummy values should be chosen an order of magnitude higher than the actual motion of the system. Furthermore, covariances smaller than the suggested will constrain the estimates too much and may lead to erroneous results. On the other hand, if too high covariances are set, the dummy measurement will not be able to properly restrict the drift on the estimates [19].

In order to include the displacement dummy measurements in the AKF algorithm, some definitions must be updated. The measurement matrix has to include information about displacement dummy measurements in Eq. 18,

$$\mathbf{H_T^\star} = \begin{bmatrix} \mathbf{H}^\star \\ \mathbf{H_{dm}} \end{bmatrix}. \tag{20}$$

Furthermore, the sensor outputs vector must contain the displacement dummy measurements values, $\mathbf{y_{dm}}$, which are zero displacement,

$$\mathbf{y_T} = \begin{Bmatrix} \mathbf{y} \\ \mathbf{y_{dm}} \end{Bmatrix} = \begin{Bmatrix} \mathbf{y} \\ 0 \end{Bmatrix}, \tag{21}$$

and the measurement covariance matrix must include the dummy measurements covariance, as follows,

$$\mathbf{R_T} = \begin{bmatrix} \mathbf{R_v} & 0 \\ 0 & \mathbf{R_{dm}} \end{bmatrix}. \tag{22}$$

Naets et al. [19] point out that, due to the relatively large uncertainty on these dummy measurements, they will not contribute considerably to the fast estimation, typically required in force estimation for on-line control tasks. However, they will prevent the long-term drift created by the force estimation based on only acceleration measurements. In fact, since the objective of the present work is to estimate a point force rather than control a system, a fast estimation is not required.

3 Validation

In the present work, the capacity of the AKF-DM algorithm to predict a random in time point force applied on a cantilevered mounted structure is tested. In the following subsections the test apparatus and the used

instrumentation are described. Furthermore, the results of the EMA procedure are presented and used to represent the system in the modal space. Subsequently, the values for the process noise covariance matrix and input covariance matrix are set, while the dummy measurements covariance values are tuned. Finally, results on force identification are presented.

3.1 Instrumentation and section - model

The stainless steel structure (386 mm length, 19 mm diameter), shown in Fig. 1, has been manufactured in order to allow the installation of the instruments that will sense the structure vibration which are, presently, due to the external point force. In this manner, the structure is instrumented with four piezolectric uniaxial accelerometers model 352A24 with broadband resolution of 0.002 m/s^2 RMS (0.0002 g RMS), from PCB Piezotronics. They are installed at positions A1 (185 mm from fixed end) and A2 (345 mm) with sensing axes perpendicular to each other so that they can measure vibration in x and y coordinates.

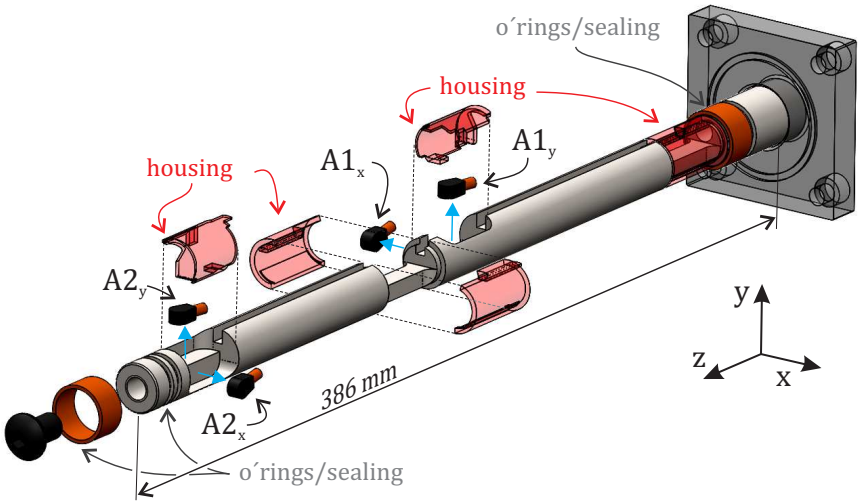

Figure 1: Instrumented cylinder.

After the sensors are installed, four 3D printed housing components are mounted on the structure, as shown in Fig. 1, in order to provide a uniform cylindrical profile. Furthermore, the structure is coated with a heat shrink tube, which is devoted to isolate the instruments from liquid when in-flow tests are performed. Although the present tests are performed in air, it was decided to maintain the heat shrink tube since it belongs to the actual structure design. It is worth mentioning that the inclusion of the mentioned coating must increase the system effective damping. Conversely, stiffness and inertia are expected to remain the same. Two aluminum rings are used to compress the o-rings mounted at the end and close to the clamping edge, and a stainless steel bolt is used to compress the heat shrink tube against the structure tip, adding some redundancy to the sealing of the instrumentation compartments.

The structure is mounted in cantilever on a section-model that represents an actual heat exchanger, whose dimensions (381 mm long and 95 mm width) and its lateral walls have been manufactured identical to the original test section. In this manner, the mounting and boundary conditions are as close as possible to those found in the actual tube bundle; the only difference being the absence of the remainder tubes that would prevent the shaker installation. Furthermore, this configuration facilitates tests with force aligned to y coordinate, however tests with force applied in x coordinate require the tube to be rotated 90° and reinstalled to allow the positioning of the shaker.

The structure is excited with an electrodynamic shaker model K2007E01 from Modal Shop, which is mounted at point A2 in order to allow collocated measurements since, as reported by Lourens et al. [16], more accurate results can be obtained with the AKF algorithm. Force is measured with a force transducer model Y208C01 from PCB Piezotronics, it is set next to the shaker (rather than the structure) in order to avoid contact with water in further experimental campaigns. The described set-up is shown in Fig. 2.

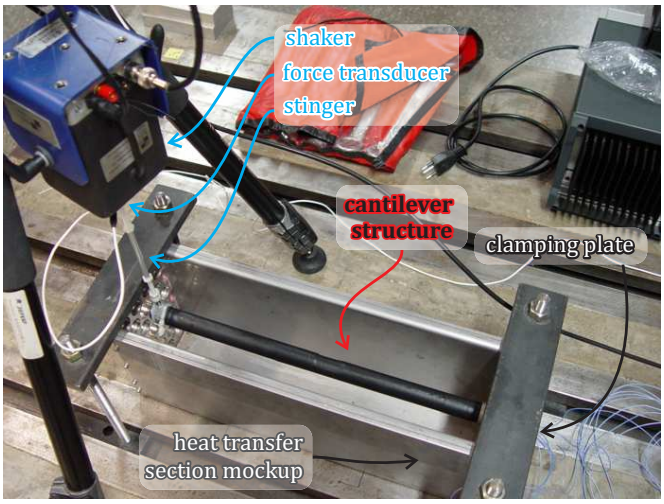

Figure 2: Experimental set-up for tests in water with electrodynamic shaker mounted at point A2.

Data is acquired with a SCADAS Mobile system running Siemens Test.Lab. The authors have devised the methodology for data acquisition and signal processing based on the form that these results are typically presented in the recent literature as well as the qualitative evolution of the data during the initial runs. Based on these criteria, acceleration and strain were measured in periods of 2 s, with a sampling frequency of 4096 Hz and a resolution of 0.5 Hz. Moreover, the obtained FRFs are the result of 30 linear averages.

3.2 System identification

The system dynamic behavior can be approximated via experimental identification. It is worth mentioning that a successful identification is very valuable since it can reduce the dependence of state estimation on the modeling of system (plant) uncertainties.

In the present study, EMA techniques are used to identify and represent the cantilevered structure described above. For this, the structure is excited at point A2 and responses are measured at points A1 and A2 since the structure design is intended to induce a 2 DOF behavior in the low frequency range, below 500 Hz. After acquiring the FRFs, the data post processing comprises two stages: (i) the poles and damping ratios are estimated via Least Squares Complex Exponential (LSCE) method, and (ii) residues and mode shapes coefficients are estimated via Least Squares Frequency Domain (LSFD) method.

This analysis is performed in the 0 - 500 Hz frequency bandwidth, which presents the two expected resonance frequencies, as seen in Fig. 3. This process is performed for x and y coordinates, according to the system coordinates in Fig. 1. The undamped natural frequencies, damping ratios and modal vectors are shown in Tab. 1. The modal vectors shown in these tables have been normalized according to the unity modal mass criterion.

As it can be seen from values in Tab. 1, the natural frequencies in x coordinate are distinct from those in y coordinate, which is intentional and due to the structure design, as discussed before. Moreover, in order to check the hypothesis of proportionally damped structure, mode complexity indicators such as Modal Phase Collinearity (MPC) and Mean Phase Deviation (MPD) are included in Tab. 1 for each calculated mode. Considering that for real modes MPC approaches to unity and MPD scatter value should be zero, it can be

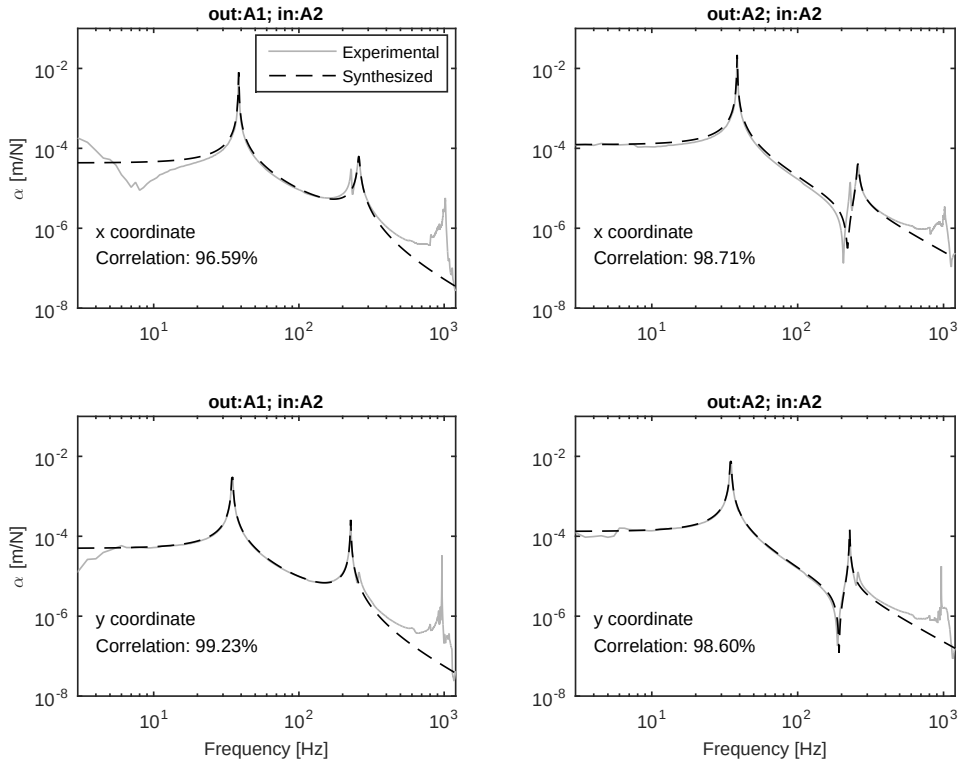

Figure 3: Experimental and synthesized receptance FRFs in x and y coordinates.

said that calculated mode shapes are normal modes, thus proportional damping is a good approximation for the present study.

The synthesized and experimental receptance FRFs are compared and shown in Fig. 3. As it can be seen from these FRFs, the models have been truncated to represent only the first two modes in each direction, since acceleration is measured only at two distinct points. Furthermore, as it can be noticed, there is some cross sensitivity, that is, the accelerometers in A1 and A2 in x coordinate are also sensing a little portion of the tube vibration in y coordinate and vice versa. This must be related to manufacturing imperfections in the surfaces where the accelerometers are installed as well as on the fixturing of the sensors themselves. This effect is more accentuated in x than in y coordinate. Despite this, the identified system, represented by the synthesized FRFs, presents high correlation with experimental data for the frequency bandwidth in which the EMA algorithms are implemented [2].

[2]Correlation values are obtained from LMS Test.Lab - Modal Analysis module.

Parameter		**x** coordinate		**y** coordinate	
		Mode 1	**Mode 2**	**Mode 1**	**Mode 2**
f [Hz]		38.4	258.4	34.7	227.1
ζ [%]		0.26	1.32	0.52	0.42
ψ	A1	9.81×10^{-1}	-2.61×10^{0}	9.96×10^{-1}	-2.78×10^{0}
	A2	2.67×10^{0}	1.68×10^{0}	2.50×10^{0}	1.60×10^{0}
MPC		1	1	1	1
MPD		1×10^{-14}°	3×10^{-15}°	3×10^{-15}°	3×10^{-15}°

Table 1: EMA results in x and y coordinates.

3.3 Covariance matrices

The present Kalman filtering implementation entails in tuning of process, input and dummy measurements covariances, whereas measurement covariance related to accelerometers is obtained from calibration tests or provided by the instrument manufacturer.

The process noise covariance matrix, $\mathbf{R}_{\mathbf{w}}^{\star}$, as defined in Eq. 17, contains information about the uncertainty on the proposed model for the system and input force. Since the system has been identified in situ via EMA techniques in section 3.2, it can be assumed as exact [19] in the analyzed frequency bandwidth even though the modal model was truncated for its first two vibration modes. Assuming an exact system model the tuning variables related to process covariance can be eliminated and all the uncertainty can be charged to the unknown covariance. This criterion agrees with that proposed by Berg and Keith Miller [20], who used very low covariance for the system in comparison to the input force covariance. On the other hand, the input force is totally unknown. Therefore, for tests in both coordinates, a very low covariance values in $\mathbf{R}_{\mathbf{w}}$ are assumed, given in the form:

$$\mathbf{R}_{\mathbf{w}} = \begin{bmatrix} R_{\dot{\xi}} & 0 \\ 0 & R_{\ddot{\xi}} \end{bmatrix}, \tag{23}$$

with

$$R_{\dot{\xi}} = 1(\text{m/s})^2, \qquad R_{\ddot{\xi}} = 1(\text{m/s}^2)^2. \tag{24}$$

Moreover, it is worth noting that all the covariance matrices in this section are assumed as diagonal matrices since disturbances are mutually uncorrelated. Furthermore, the input covariance matrix $\mathbf{R}_{\mathbf{z}}$ is defined as:

$$\mathbf{R}_{\mathbf{z}} = \begin{bmatrix} R_{\dot{u}1} & 0 \\ 0 & R_{\dot{u}2} \end{bmatrix}. \tag{25}$$

where $R_{\dot{u}1} = 0$ N^2 because no force was applied at point A1 and $R_{\dot{u}2}$ is tuned and set equal to 4×10^{10} N^2. According to Naets et al. [19], $R_{\dot{u}2}$ must be a high value in order to avoid inhibiting the estimation. This value has been used for both directions.

The instruments covariance, $\mathbf{R}_{\mathbf{T}}$, given by Eq. 22, contains information about the uncertainty on the dummy measurements, whose matrix covariance is defined by

$$\mathbf{R}_{\mathbf{dm}} = \begin{bmatrix} R_{dm1} & 0 \\ 0 & R_{dm2} \end{bmatrix}, \tag{26}$$

where R_{dm1} and R_{dm2} are tuning variables chosen an order of magnitude higher than the actual motion of the system [19]. In this sense, estimates for displacement are obtained by using the model identified in section 3.2 and simulating its time response to the measured force applied on A2. Thus, for the present study it is assumed that $R_{dm1} = R_{dm2} = 1 \times 10^{-5}$ m^2, which are maintained for tests in both coordinates.

Regarding the accelerometers covariance, $\mathbf{R}_{\mathbf{v}}$, it is given by

$$\mathbf{R}_{\mathbf{v}} = \begin{bmatrix} R_1 & 0 \\ 0 & R_2 \end{bmatrix}, \tag{27}$$

where R_1 and R_2 correspond to the covariance of accelerometers in A1 and A2, respectively, which were obtained via calibration and are detailed in Tab. 2.

Table 2: Accelerometers covariance in (m/s^2)^2.

Point	x **coordinate**	y **coordinate**
A1	40×10^{-4}	33×10^{-4}
A2	42×10^{-4}	22×10^{-4}

3.4 Results on force identification

The results on the prediction of a random in time point force via AKF-DM algorithm are discussed in this section. Since the force is predicted via a recursive type algorithm, which is based on actual acceleration measurements for its updating, it is necessary to define the time step for its implementation. It is convenient to define the same sampling time used for data acquisition as the time step for system discretization, this is $\Delta t = 2.4414 \times 10^{-4}$ s.

First, a comparison between the predicted and measured forces in the x coordinate is shown in Fig. 4. In order to do that, the results are presented in a time window of 2 s with detailed views in two time lapses of 0.04s. These time lapses are taken at the beginning and at the end of the complete window. As it can be noticed from these time lapses, the AKF-DM algorithm is able to predict the actual force in a relatively good manner based only on acceleration measurements and by introducing the displacement dummy measurements. In the same manner, as it can be noticed from Fig. 5, predicted forces for the y coordinate are in good agreement with measurements. For results in both coordinates, it can be seen that predicted forces differ slightly from the actual values at the beginning of the time window, however, these differences decrease rapidly.

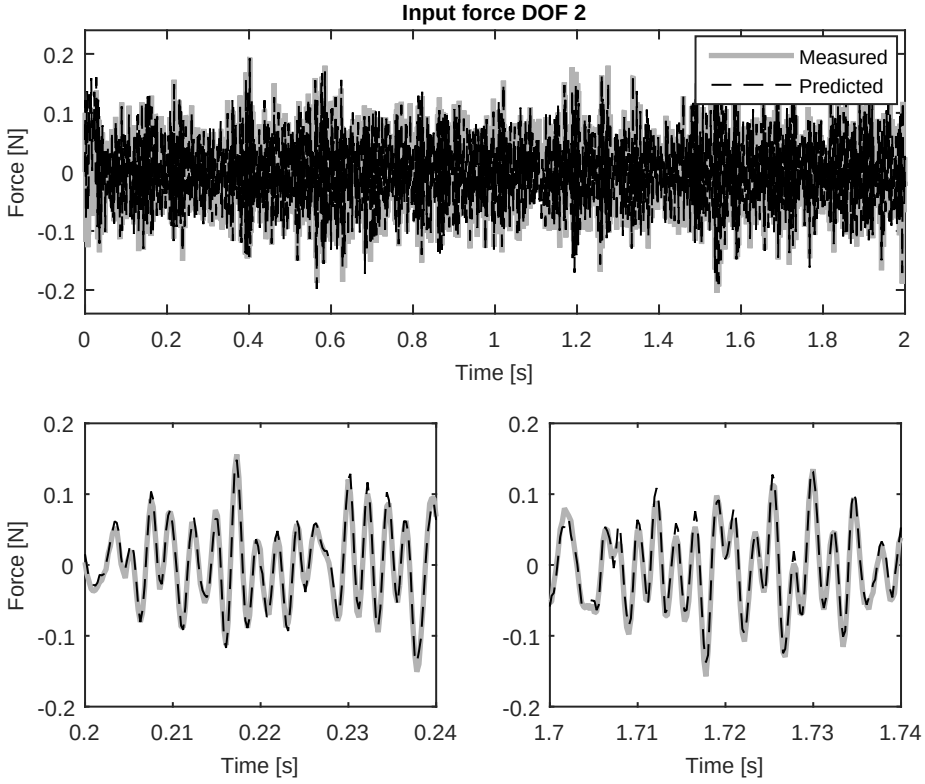

Figure 4: Measured and estimated force at DOF 2 in x coordinate shown for a complete time window and in detail for two distinct time lapses.

In general, it can be said that forces predicted via AKF-DM are in good agreement with the measurements. However, it must be noted that this result cannot be completely extrapolated for the other state variables. In other words, predicted ξ and $\dot{\xi}$ may present distinct behavior if compared with values estimated via numerical simulation in MATLAB ®, as shown, for example, for the x coordinate in Fig. 6. These differences can be better analyzed when comparing the Power Spectrum Densities (PSD) of displacement at each instrumented point, which is shown in Fig. 6. As it can be noticed, the main difference between simulated and predicted values is that the former presents a higher peak amplitude at the resonance frequency, which makes sense with the results presented in time domain.

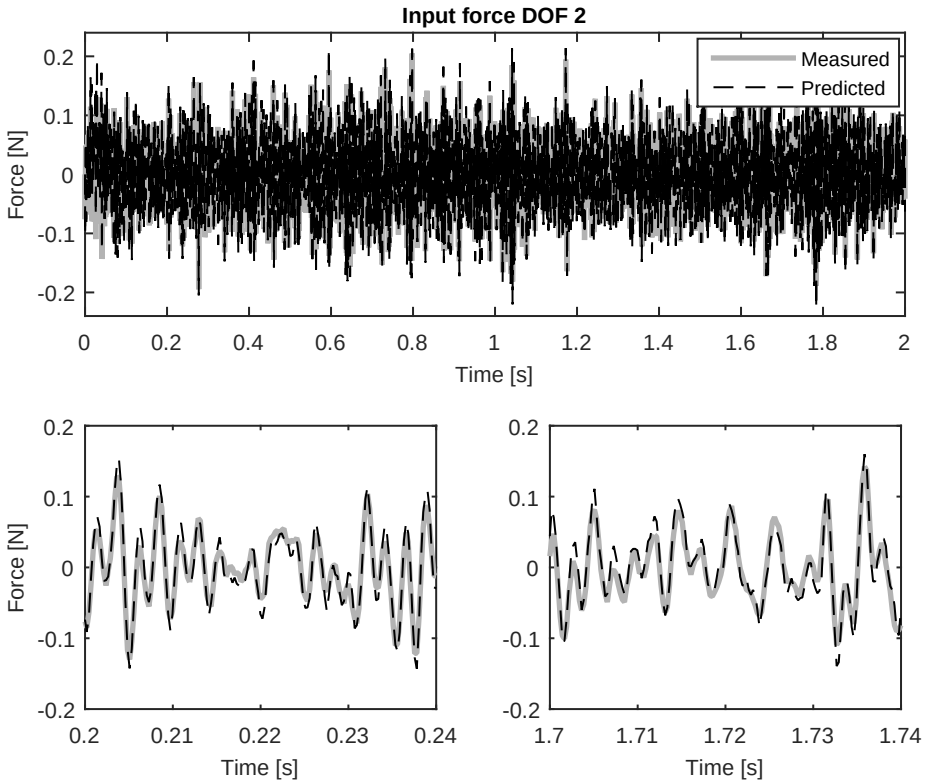

Figure 5: Measured and estimated force at DOF 2 in y coordinate shown for a complete time window and in detail for two distinct time lapses.

4 Conclusions

The ability of the AKF-DM algorithm for predicting a random in time, point force, applied on a cantilever structure was checked. For this, the KF was tuned at hand.

The comparison between experimental and predicted force time histories showed good agreement in x and y coordinates. Hence, it can be said that the AKF-DM algorithm is capable of predicting random point forces. However, it was seen that the AKF-DM algorithm fails to predict the other state variables; *i.e.* displacement and velocity.

Based on these results, further works can be proposed on the study of two-phase flow-induced forces via KF based techniques. These studies, currently under investigation, will present a set of more complex surrounding conditions, *e.g.* flow velocity and buffeting forces due to two-phase flow.

Acknowledgements

The authors acknowledge the financial assistance of the Brazilian National Council for Scientific and Technological Development - CNPq (grant numbers 481044/2010-8 and 307369/2013-7) and the doctoral scholarship awarded to the first author by CAPES Foundation.

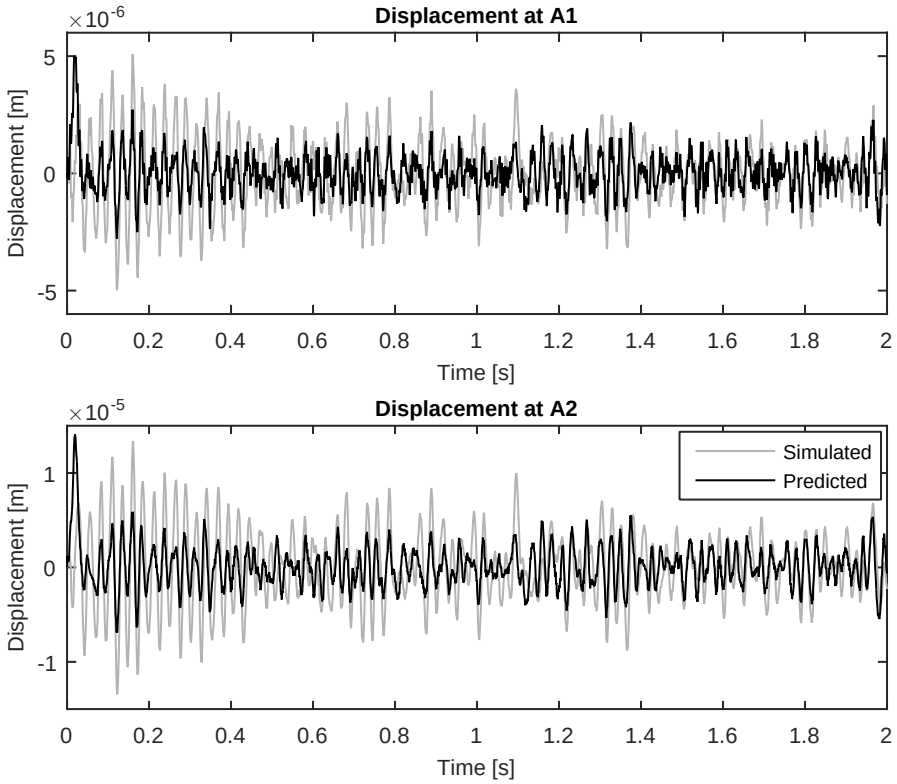

Figure 6: Simulated and predicted displacements in x coordinate

References

[1] F. T. Kanizawa, G. Ribatski, *Two-phase flow patterns across triangular tube bundles for air-water upward flow*, International Journal of Multiphase Flow, Vol. 80, Elsevier (2016), pp. 43-56.

[2] S. J. Green, G. Hetsroni, *PWR steam generators*, International Journal of Multiphase Flow, Vol. 21, No. 1, Pergamon (1995), pp. 1-97.

[3] G. Noghrehkar, M. Kawaji, A. Chan, *Investigation of two-phase flow regimes in tube bundles under cross-flows conditions*, International Journal of Multiphase Flow, Vol. 25, Pergamon (1999), pp. 857-874.

[4] M. J. Pettigrew, C. E. Taylor, *Vibration analysis of shell and tube heat exchangers: an overview - part 2. vibration response, fretting wear, guidelines*, Journal of Fluids and Structures, Vol. 18, Elsevier (2003), pp. 485-500.

[5] M. J. Pettigrew, C. E. Taylor, *Two-phase flow induced vibration: An overview*, Journal of Pressure Vessel Technology, Vol. 116, American Society of Mechanical Engineers (1994), pp. 233-253.

[6] M. J. Pettigrew, C. E. Taylor, *Vibration analysis of shell and tube heat exchangers: an overview - part 1. flow damping, fluidelastic instability*, Journal of Fluids and Structures, Vol. 18, Elsevier (2003), pp. 469-489.

[7] S. Kaneko, T. Nakamura, F. Inada, M. Kato, *Flow Induced Vibrations: Classifications and Lessons from Practical Experiences*, Elsevier (2008).

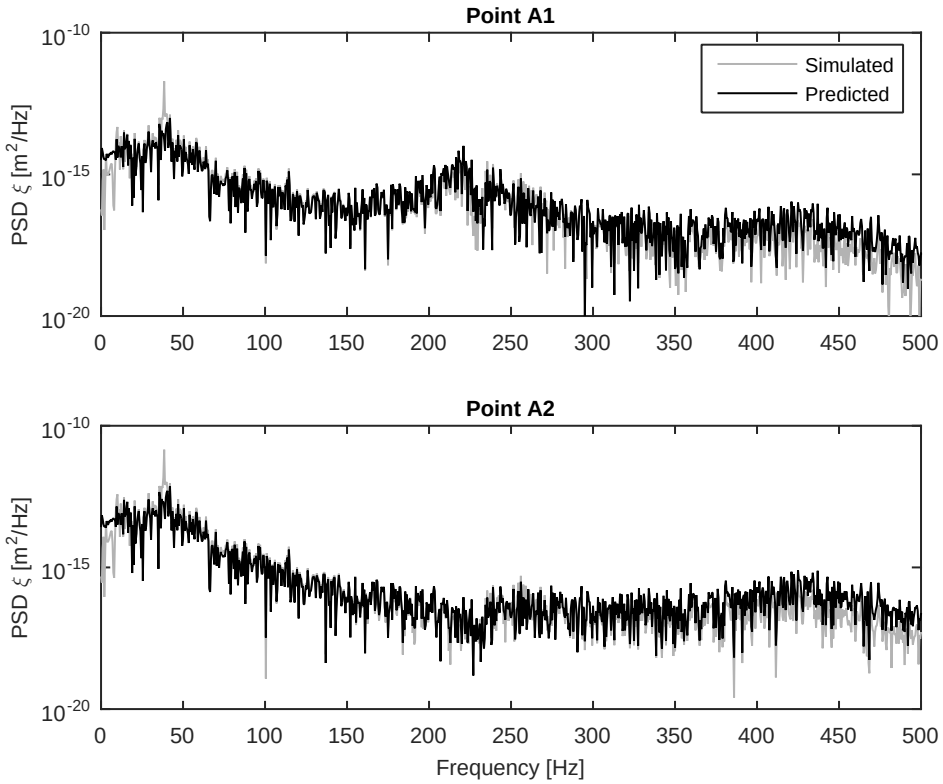

Figure 7: PSDs of simulated and predicted displacements in x coordinate

[8] M. J. Pettigrew, C. E. Taylor, V. P. Janzen, T. Whan, *Vibration behavior of rotated triangular tube bundles in two-phase cross flows*, Journal of Pressure Vessel Technology, Vol. 124, American Society of Mechanical Engineers (2002), pp. 144-153.

[9] M. J. Pettigrew, L. N. Carlucci, C. E. Taylor, N. Fisher, *Flow-induced vibration and related technologies in nuclear components*, Nuclear Engineering and Design, Vol. 131, Elsevier (1991), pp. 81-100.

[10] R. Álvarez - Briceño, F. T. Kanizawa, G. Ribatski, L. P. R. de Oliveira, *Updated results on hydrodynamic mass and damping estimations in tube bundles under two-phase crossflow*, International Journal of Multiphase Flow, Vol. 89, Elsevier (2017), pp. 150-162.

[11] R. Álvarez - Briceño, F. T. Kanizawa, G. Ribatski, L. P. R. de Oliveira, *Validation of turbulence induced vibration design guidelines in a normal triangular tube bundle during two-phase crossflow*, Journal of Fluids and Structures, Vol. 76, Elsevier (2018), pp. 301-318.

[12] R. Álvarez - Briceño, L. P. R. de Oliveira, F. T. Kanizawa, G. Ribatski, *Flow Induced Vibrations in Tube Bundles under Crossflow. Encyclopedia of Two-Phase Heat Transfer and Flow III: Macro and Micro Flow Boiling and Numerical Modeling Fundamentals. 1ed.*, World Scientific Publishing Co. Pte. Ltd., v. 4, p. 251-334 (2018).

[13] E. Wilson, *Virtual sensor technology for process optimization*, in *Proceedings of the Symposium on Computers and Controls in the Metals Industry in Iron and Steel Society, Baltimore, Maryland, 1997*, USA (2001).

[14] J. Croes, *Virtual sensing in mechatronic systems. State estimation using system level models*, PhD thesis, Katholieke Universiteit Leuven, Leuven (2017).

[15] F. Naets, J. Croes, W. Desmet *An online coupled state/input/parameter estimation approach for structural dynamics*, Computer methods in applied mechanics and engineering, Vol. 283, Elsevier (2015), pp. 1167-1188.

[16] E. Lourens, E. Reynders, G. De Roeck, G. Degrande, G. Lombaert, *An augmented Kalman filter for force identification in structural dynamics*, Mechanical Systems and Signal Processing, Vol. 27, Elsevier (2012), pp. 446-460.

[17] R. E. Kalman, *A new approach to linear filtering and prediction problems*, Journal of Basic Engineering, Vol. 82, American Society of Mechanical Engineers (1960), pp. 35-45.

[18] R. E. Kalman, R. S. Bucy, *New results in linear filtering and prediction theory*, Journal of Basic Engineering, Vol. 83, American Society of Mechanical Engineers (1961), pp. 95-108.

[19] F. Naets, J. Cuadrado, W. Desmet, *Stable force identification in structural dynamics using Kalman filtering and dummy measurements*, Mechanical Systems and Signal Processing, Vol. 50 - 51, Elsevier (2015), pp. 235-248.

[20] J. C. Berg, A. Keith Miller, *Force estimation via Kalman filtering for wind turbine blade control*, *Proceedings of the IMAC - XXVIII, Jacksonville, Florida, USA, 2010*, USA (2010).

[21] N. Maia, J. Silva, *Theoretical and Experimental Modal Analysis*, 1st ed., Research Studies Press LTD., Hertfordshire (1998).

[22] L. P. R. de Oliveira, P. S. Varoto, P. Sas, W. Desmet, *A state-space modeling approach for active structural acoustic control*, Shock and Vibration, Vol. 16 (6), Hindawi (2009), pp. 607-621.

[23] G. Franklin, J. D. Powell, M. Workman, *Digital control of dynamic systems*, Ellis - Kagle Press, Addison-wesley Menlo Park, CA (1998).

[24] M. L. J. Hautus, *Stabilization controllability and observability of linear autonomous systems*, *Proceedings of Indagationes Mathematicae, Eindhoven, The Netherlands, 1970*, Eindhoven (1970).

[25] C. -K. Ma, P. -C. Tuan, D. -C. Lin, C. -S. Liu, *A study of an inverse method for estimation of impulsive loads*, International Journal of Systems Science, Vol. 29, Taylor & Francis (1998), pp. 663-672.

[26] C. -K. Ma, J. -M. Chang, D. -C. Lin, *Input forces estimation of beam structures by an inverse method*, Journal of Sound and Vibration, Vol. 259 (3), Elsevier (2003), pp. 387-407.

[27] J. J. Liu, C. -K. Ma, I. C. Kung, D. -C. Lin *Input force estimation of a cantilever plate by using a system identification technique*, Computer Methods in Applied Mechanics and Engineering, Vol. 190, Elsevier (2000), pp. 1309-1322.

[28] J. -S. Hwang, A. Kareem, W. -J. Kim, *Estimation of modal loads using structural response*, Journal of Sound and Vibration, Vol. 326 (3-5), Elsevier (2009), pp. 522-539.

[29] D. Simon, *Optimal State Estimation: Kalman, H_∞ and Nonlinear Approaches*, John Wiley and Sons, New York (2006).

[30] W. M. Wonham, *On a matrix Riccati equation of stochastic control*, SIAM Journal on Control, Vol. 6 (4), SIAM (1968), pp. 681-697.

[31] V. Kucera, *A contribution to matrix quadratic equations*, IEEE Transactions on Automatic Control, Vol. 17 (3), IEEE (1972), pp. 344-347.

[32] E. N. Chatzi, C. Fuggini, *Structural identification of a super-tall tower by gps and accelerometer data fusion using a multi-rate kalman filter*, *Life-Cycle and Sustainability of Civil Infrastructure Systems: Proceedings of the Third International Symposium on Life-Cycle Civil Engineering (IALCCE12), Vienna, Austria, 2012*, Vienna (2012).